Effect of Stress on Switched Reluctance Motors: A Magneto-Elastic Finite-Element Approach Based on Multiscale Constitutive Laws

Laurent Bernard[1], Xavier Mininger[1], Laurent Daniel[1], Guillaume Krebs[1], Frédéric Bouillault[1], and Mohamed Gabsi[2]

[1]LGEP (CNRS (UMR 8507); SUPELEC; Univ Paris-Sud; UPMC Paris 6), F-91192 Gif sur Yvette Cedex, France
[2]SATIE (ENS Cachan; CNRS (UMR 8029); UniverSud), F-94230 Cachan, France

The design of electromagnetic devices submitted to high mechanical stress is a growing issue and requires consequently appropriate modeling tools. We propose in this paper to implement a multiscale model for magneto-elastic behavior into a finite-element code. The 2-D magneto-elastic constitutive law is derived from a multiscale model based on a local energetic approach. The method is applied to study the effect of stress on the magnetic behavior of a switched reluctance motor. This work provides a finite-element tool for the modeling of the effect of multiaxial stress on electrotechnical devices.

Index Terms—**Effect of stress, electrical machines, finite-element method, magneto-elasticity, multiscale modeling.**

I. Introduction

MAGNETIC materials in electrical machines or actuators are submitted to multiaxial mechanical loadings. These stress states can be inherited from forming and assembly processes (cutting, stacking, welding, etc.) or appear in use (magnetic forces, inertial forces, etc.). On the other hand, stress significantly modifies the magnetic and magnetostrictive behavior [1]. The increase of manufacturing constraints (for cost reduction) and operating constraints (for cost reduction or compacity purpose) emphasizes the need for appropriate coupled modeling tools in the design of electromagnetic systems. One possible choice is the introduction of coupled constitutive laws into finite-element modeling. Unfortunately, most magneto-elastic models are restricted to uniaxial mechanical loadings (e.g., [2]–[5]). Some authors proposed to define a magneto-elastic equivalent stress, namely a (fictive) uniaxial stress that would change the magnetic behavior in a similar manner than the multiaxial one [6]–[10]. These approaches can be suited for certain particular multiaxial configuration of stress but did not succeed in giving a general description of the effect of stress on magneto-elastic behavior. Fully multiaxial magneto-elastic models, based on an energetic approach, have been proposed for single crystals [11] and for single and poly-crystalline media, including the effect of crystallographic texture [12]–[14]. The implementation of the latter models into a finite-element simulation still leads to dissuasive computational times for engineering design applications. For an application of single crystals under uniaxial loadings, Graham *et al.* [15] proposed a finite-element code using look-up text files containing scalar values of magnetostriction and magnetic field depending on stress and magnetic induction amplitudes (assuming the uniaxial stress to be parallel to the magnetic induction). They used the Armstrong model [16] to build these files. If a more general configuration is to be treated, such as a multiaxial stress combined to a magnetic field not aligned with a principal stress direction, the number of inputs for the precalculated data file is quickly increasing. We propose in this paper to define a simplified bi-dimensional version of the multiscale approach proposed in [14] and to implement it directly into a coupled magneto-mechanical numerical code. This approach provides an original finite-element approach for the modeling of the effect of multiaxial stress on electrotechnical devices. It is applied to the calculation of the magnetic field in the rotor of a switched reluctance motor submitted to different sources of mechanical stress.

Manuscript received July 22, 2010; revised October 25, 2010 and February 25, 2011; accepted April 12, 2011. Date of publication April 21, 2011; date of current version August 24, 2011. Corresponding author: L. Bernard (e-mail: laurent.bernard@lgep.supelec.fr).

Color versions of one or more of the figures in this paper are available online at http://ieeexplore.ieee.org.

Digital Object Identifier 10.1109/TMAG.2011.2145387

II. Local Magneto-Elastic Constitutive Law

The local magneto-elastic constitutive law is derived from the multiscale approach detailed in [13] and [14]. This model is based on the description of the magnetic material as a set of magnetic domains with known magnetization (M_s) and random orientation. The local free energy of a magnetic domain is expressed as the sum of three contributions: the magneto-static, the magneto-crystalline anisotropy, and the elastic energies. The magneto-elastic behavior is obtained by defining the volumetric fraction of a domain with a given magnetization through the use of a Boltzmann probability function. This model provides a multiaxial description of the magneto-elastic behavior and includes effects such as the dependence of magnetostriction strain on stress or crystallographic texture effects. However, due to computation time constraints, this approach cannot be easily implemented into motor design numerical tools. We propose to define a simplified version of the multiscale model (MSM) that allows to reduce by a factor greater than 1000 the computational burden due to the coupled constitutive law. The simplified model uses additional assumptions and gets close to Armstrong model [11].

The model is reduced to a 2-D configuration. The material is assumed to be a collection of magnetic domains randomly oriented. The model defines the probability of existence of a domain oriented along a given direction $\vec{\alpha}$. The local potential energy W_α of the material is written using the same principle as the full MSM (1) [13]. It defines the magneto-static and elastic contributions, (2) and (3). A macroscopic anisotropy can result from the combination of crystalline anisotropy and crystallographic texture. This macroscopic anisotropy can be described through an anisotropy energy term (e.g., in (4) for a uniaxial

anisotropy along direction $\vec{\beta}$, K being a constant to be identified). If we assume macroscopic isotropy, this term vanishes

$$W_\alpha = W_\alpha^{mag} + W_\alpha^{el} + W_\alpha^{an} \quad (1)$$
$$W_\alpha^{mag} = -\mu_0 \vec{H}.\vec{M}_\alpha \quad (2)$$
$$W_\alpha^{el} = -\boldsymbol{\sigma} : \boldsymbol{\varepsilon}_\alpha^\mu \quad (3)$$
$$W_\alpha^{an} = K(\vec{\alpha}.\vec{\beta})^2. \quad (4)$$

The following 2-D definitions for the local magnetization $\vec{M}_\alpha$ and magnetostriction strain $\boldsymbol{\varepsilon}_\alpha^\mu$ are used:

$$\vec{M}_\alpha = M_s\vec{\alpha} = M_s\begin{bmatrix}\alpha_1\\ \alpha_2\end{bmatrix} \quad (5)$$
$$\boldsymbol{\varepsilon}_\alpha^\mu = \frac{3}{2}\begin{pmatrix}\lambda_{l_1}\left(\alpha_1^2-\frac{1}{3}\right) & \lambda_t\alpha_1\alpha_2\\ \lambda_t\alpha_1\alpha_2 & \lambda_{l_2}\left(\alpha_2^2-\frac{1}{3}\right)\end{pmatrix}. \quad (6)$$

μ_0 is the vacuum permeability. $\vec{H}$ and $\vec{M}_\alpha$ are the magnetic field and magnetization. $\boldsymbol{\sigma}$ and $\boldsymbol{\varepsilon}_\alpha^\mu$ are the stress and magnetostriction strain second order tensors. M_s is the saturation magnetization of the material, λ_{l_1}, λ_{l_2}, and λ_t are magnetostriction constants. Assuming an isotropic behavior, we consider $\lambda_{l_1} = \lambda_{l_2} = \lambda_t = \lambda$.

The unknown of the problem is the local magnetization direction $\vec{\alpha}$. The probability f_α for the magnetization to be in the direction $\vec{\alpha}$ is calculated using a Boltzmann type relation:

$$f_\alpha = \frac{\exp(-A_s.W_\alpha)}{\int_\alpha \exp(-A_s.W_\alpha)}. \quad (7)$$

A_s is a material parameter linked to the initial anhysteretic susceptibility χ_o [13]. Once the probability f_α is defined, the macroscopic magnetization $\vec{M}$ and magnetostriction $\boldsymbol{\varepsilon}^\mu$ are obtained thanks to an averaging operation over all possible directions:

$$\vec{M} = \langle\vec{M}_\alpha\rangle = \int_\alpha f_\alpha\vec{M}_\alpha d\alpha \quad (8)$$
$$\boldsymbol{\varepsilon}^\mu = \langle\boldsymbol{\varepsilon}_\alpha^\mu\rangle = \int_\alpha f_\alpha\boldsymbol{\varepsilon}_\alpha^\mu d\alpha. \quad (9)$$

This integration step is performed numerically using a discretization of possible orientations $\vec{\alpha}$.

The material parameters for this simplified 2-D modeling are M_s, λ, and A_s in the case of macroscopic isotropy. The parameter K, the direction of anisotropy $\vec{\beta}$ and magnetostriction parameters are to be added for a material with a macroscopic uniaxial anisotropy. The identification of these material parameters can be made by using the full 3-D MSM as a numerical testing machine in a few particular loading cases. These parameters can also be identified to fit experimental measurements. In the particular case of macroscopic isotropy, the parameter can be easily identified (see the Appendix): M_s is the saturation magnetization of the material, λ can be obtained from the macroscopic saturation magnetostriction strain λ_s of the material ($\lambda = 4\lambda_s/3$) and A_s can be deduced from the initial slope χ_0 of the anhysteretic magnetization curve under no applied stress ($A_s = 2\chi_0/(\mu_0 M_s^2)$).

The description of the material as a collection of planar domains appears quite restrictive compared to the real 3-D configuration, and we can expect the prediction of the behavior under multiaxial loadings to be less accurate than with the full 3-D MSM. Moreover crystallographic texture effect cannot be addressed accurately with the simplified model: the description of macroscopic anisotropy can only be made through a macroscopic term. We can also notice that due to the 2-D assumption, only external loadings consistent with the 2-D symmetry of the problem can be handled.

TABLE I
MATERIAL PARAMETERS USED IN THE CALCULATION

Parameter	M_s	λ_s	A_s
Value	$1.8\ 10^6$	$50\ 10^{-6}$	$1.8\ 10^{-3}$
Unit	$A.m^{-1}$	-	$m^3.J^{-1}$

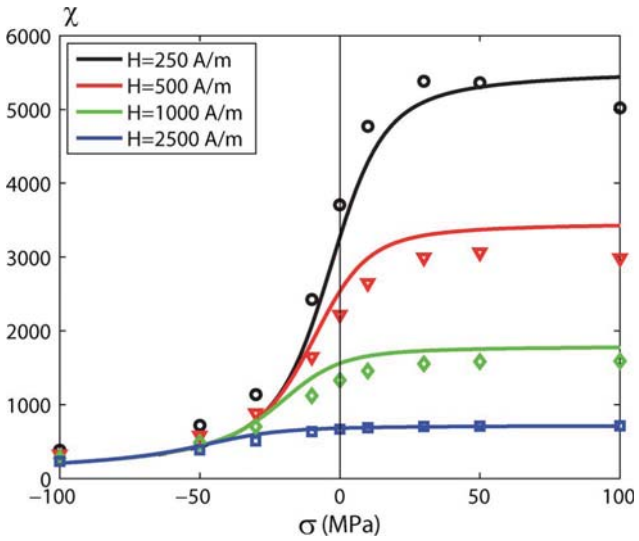

Fig. 1. Magnetic susceptibility under uniaxial mechanical stress: simplified 2-D modeling (lines) and experimental results (dots) from [10].

The material parameters used for the application presented in this paper are given in Table I and have been identified from experimental measurements on an iron-cobalt alloy [10], [17].

The evolution of the predicted susceptibility as a function of the applied stress has been plotted in Fig. 1 for different levels of magnetic field. The comparison to the experimental results excerpted from [10] is satisfying.

The magnetostrictive behavior under uniaxial stress state has also been plotted in Fig. 2 and compared to the experimental results obtained on the same material [17]. The high sensitivity of the magnetostrictive behavior to the application of stress is well captured by the 2-D model.

An example of the magnetic behavior under uniaxial stress state in the direction of the magnetic field, is given in Fig. 3, highlighting the strong effect of compressive stress on the magnetization curve.

The magneto-elastic behavior under multiaxial stress can also be defined. An illustration is given in Fig. 4 concerning the susceptibility of the material for an applied magnetic field of 250 A/m as a function of the applied bi-axial stress (σ_{11} and σ_{22} being the principal stresses with σ_{11} in the direction of the magnetic field). A compressive stress parallel to the magnetic field direction combined to a tensile stress perpendicular to the magnetic field direction results in a dramatic decrease of the material

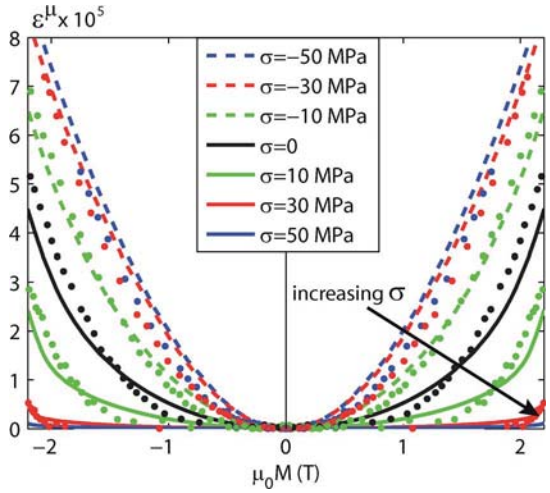

Fig. 2. Magnetostriction curve under uniaxial mechanical stress: simplified 2-D modeling (lines) and experimental results (dots) from [17].

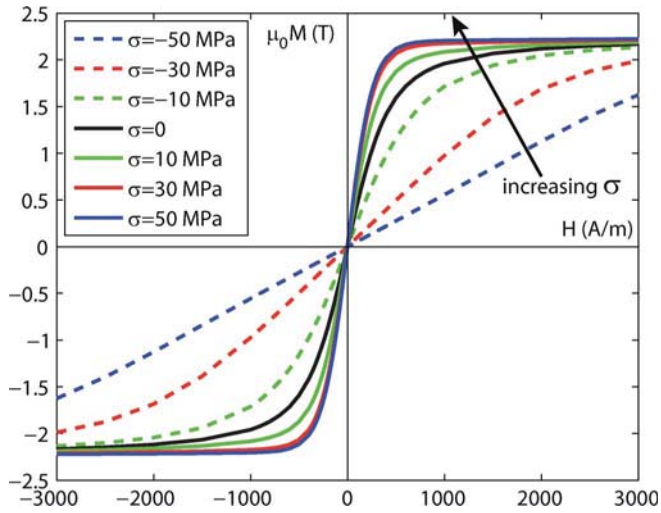

Fig. 3. Magnetization curve under uniaxial mechanical stress.

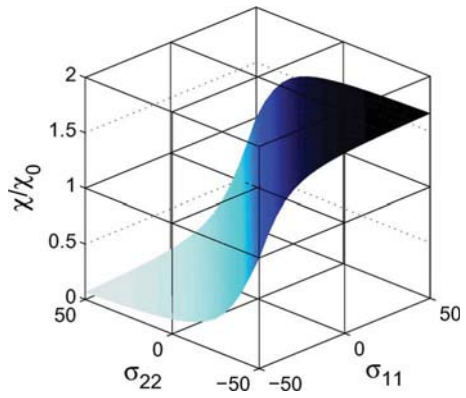

Fig. 4. Relative susceptibility in direction 1 as a function of the principal stresses σ_{11} and σ_{22} ($\mathrm{H} = 250\ \mathrm{A/m}$).

magnetic susceptibility. On the other hand a bitension mechanical loading hardly increases the susceptibility.

Fig. 5. Principle and parameters of the multiscale model (MSM).

This simplification of the full MSM allows to define the magneto-elastic response of the material with very low computational cost. This constitutive law (illustrated in Fig. 5) is then implemented into a finite-element formulation, and will be applied to each element of the mesh.

III. Finite-Element Formulation

The static finite-element model (FE) is based on classical mechanical and magnetic formulations [18]. Hysteresis and eddy-current effects are not taken into account. The mechanical problem with external forces f (see Section IV-A for more details on these forces):

$$div\boldsymbol{\sigma} = -f \tag{10}$$

is considered with the decomposition of the total strain $\boldsymbol{\varepsilon}$ into the elastic strain $\boldsymbol{\varepsilon}^e(\boldsymbol{\sigma})$ and the magnetostriction strain $\boldsymbol{\varepsilon}^\mu(\vec{H},\boldsymbol{\sigma})$:

$$\boldsymbol{\varepsilon} = \boldsymbol{\varepsilon}^e + \boldsymbol{\varepsilon}^\mu \tag{11}$$

and with the constitutive law:

$$\boldsymbol{\sigma} = [C]\boldsymbol{\varepsilon}^e \tag{12}$$

where $[C]$ is the usual stiffness tensor.[1] The total strain $\boldsymbol{\varepsilon}$ corresponds to the symmetrical part of the displacement (U) gradient:

$$\boldsymbol{\varepsilon}_{ij} = \frac{1}{2}\left(\frac{\partial U_i}{\partial x_j} + \frac{\partial U_j}{\partial x_i}\right). \tag{13}$$

The resulting mechanical formulation contains an additional term $F^\mu(\vec{H},\boldsymbol{\sigma})$, corresponding to an equivalent force due to the magneto-elastic coupling. After discretization with nodal elements, this term is expressed with

$$F^\mu(\vec{H},\boldsymbol{\sigma}) = \int_\Omega \nabla^s[C]\boldsymbol{\varepsilon}^\mu(\vec{H},\boldsymbol{\sigma})d\Omega. \tag{14}$$

∇^s is the symmetrical gradient of the shape functions, Ω the study domain, and $\boldsymbol{\varepsilon}^\mu(\vec{H},\boldsymbol{\sigma})$ is the magnetostriction strain obtained from the multiscale model.

Similarly, the magnetic scalar potential Φ formulation contains an additional term equivalent to a magnetic charge. The current sources are accounted for by the use of a term $\vec{T}_0$ in the definition of the scalar potential [19]:

$$\vec{H} = -\overrightarrow{grad}\Phi + \vec{T}_0. \tag{15}$$

The finite-element formulation is expressed in terms of magnetic scalar potential and not with the magnetic vector potential

[1]Linear elasticity and small strains are assumed.

so as to use directly the MSM model presented in Fig. 5. Indeed, the use of the vector potential would require an inversion of the magnetic part of the MSM model in order to get the convergence of the iterative process. The magnetic flux density $\vec{B}$ is defined from the magnetization $\vec{M}$:

$$\vec{B} = \mu_0(\vec{H} + \vec{M}). \tag{16}$$

Moreover, a modified fixed point (FP) iterative method is used to insure the convergence of the nonlinear problem [20]. This method provides a slow but robust convergence. The method defines a fictive permeability μ_{FP}, the algorithm convergence depending on the choice of its value. It also introduces a fictive source term $\vec{M}_{FP}(\vec{H}, \boldsymbol{\sigma})$ such that

$$\vec{B} = \mu_{FP}(\vec{H} + \vec{M}_{FP}). \tag{17}$$

Maxwell's flux conservation is written:

$$div(\mu_{FP}\overrightarrow{grad}\Phi) = div\left(\mu_{FP}\left(\vec{M}_{FP}(\vec{H}, \boldsymbol{\sigma}) + \vec{T}_0\right)\right). \tag{18}$$

From (16) and (17), $\vec{M}_{FP}(\vec{H}, \boldsymbol{\sigma})$ is updated at each iteration using the magnetization obtained with the MSM. Thus, the coupling term in the magnetic formulation is finally

$$Q^{\mu}(\vec{M}_{FP}) = \int_{\Omega} \mu_{FP}\nabla^m \vec{M}_{FP}(\vec{H}, \boldsymbol{\sigma}) d\Omega \tag{19}$$

with ∇^m the gradient of the shape functions. The coupled system is then defined by

$$\begin{cases} [S](\Phi) = (Q^{\mu}(M_{FP})) + \left(Q^0(T^0)\right) \\ [K](U) = (F) + (F^{\mu}(\boldsymbol{\varepsilon}^{\mu})) \end{cases} \tag{20}$$

with S and K respectively the magnetic and mechanical stiffness matrices, U the displacement field, and F the external forces. Finally, the resolution of the coupled nonlinear system (20) is based on the algorithm presented in Fig. 6: values of magnetization and magnetostriction strain are updated using the MSM model at each step i for each element of the mesh, until the error criterion e falls below e_c. In this work a value of 1.10^{-4} has been used for e_c. For the calculations presented hereafter, the typical number of iterations to convergence is about 15, corresponding to a total computational time of a few minutes on a standard computer. The number of iterations is directly linked to the nonlinearity of the problem. For low current sources, the material behavior is almost linear and the computation converges quickly. The computational cost is getting higher close to saturation.

IV. Application to the Rotor of a Switched Reluctance Motor

The modeling scheme has been applied to the calculation of the magnetic induction in the rotor of a high-speed switched reluctance motor (SRM). Indeed thanks to their passive rotor SRM are well-adapted for high speed applications, leading to high stress level in the rotating part. The considered configuration is given in Fig. 7. The radius of the rotor is $R = 34\,\mathrm{mm}$ and the air gap is 0.4 mm. The electrical excitation is chosen considering the conjunction configuration in order to have an induction in the tooth corresponding to the beginning of the magnetic saturation (about 1.4 T for the considered material). In the following, when the conjunction configuration is considered, only one quarter of the machine is represented taking advantage of the symmetries.

$i \leftarrow 1$;
$e \leftarrow 1$; $\Phi^0 \leftarrow 0$;
$e_c \leftarrow 1.10^{-4}$; $U^0 \leftarrow 0$;
While $(e \geq e_c)$ **do**
  $[(M^i), (\boldsymbol{\varepsilon}^{\mu i})] = MSM(\vec{H}^{i-1}, \boldsymbol{\sigma}^{i-1})$;
  $M^i_{FP} = (\frac{\mu_0}{\mu_{FP}} - 1)H^{i-1} + \mu_0 M^i$;
  $[S^{FP}](\Phi^i) = (Q^{\mu}(M^i_{FP})) + Q^0(T^0)$;
  $[K](U^i) = (F) + (F^{\mu}(\boldsymbol{\varepsilon}^{\mu i}))$;
  $e = \frac{|U^i - U^{i-1}|}{|U^i|} + \frac{|\Phi^i - \Phi^{i-1}|}{|\Phi^i|}$;
  $i \leftarrow i + 1$;
done

Fig. 6. Modified fixed-point algorithm; i stands for the iteration number, MSM for the multiscale model.

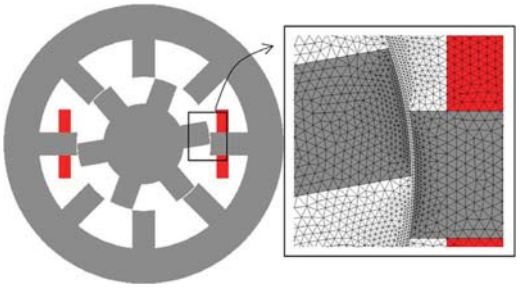

Fig. 7. Switched reluctance motor 2-D mesh.

A. Mechanical Loading

Several sources of external forces have been considered. A distinction has been made between initial forces (inherited from manufacturing process) and operating forces (appearing in use).

1) Operating Forces: Three sources of operating stress have been identified.

Incompatibility stresses arise from the magnetostriction strain in the whole machine. An upper bound for the elastic energy corresponding to these incompatibility stresses is given by the knowledge of the magnetostriction strain. This upper bound would correspond to infinitely rigid boundary conditions:[2]

$$(\boldsymbol{\sigma} : \boldsymbol{\varepsilon}^e)^{incomp} \leq \max(\boldsymbol{\varepsilon}^{\mu} : C : \boldsymbol{\varepsilon}^{\mu}). \tag{21}$$

The calculated values of this energy correspond to stress levels lower than 7 MPa if considering tensile stress. This value, overestimating the real configuration, is very low compared to the level of the other operating stresses. This term will be neglected in the following.

Stresses induced by magnetic forces are then considered. A computation with no mechanical stress is done to get the magnetic state of the whole machine. Local forces are computed at

[2]We then consider $\boldsymbol{\varepsilon}^e = -\boldsymbol{\varepsilon}^{\mu}$ so that the total strain is zero.

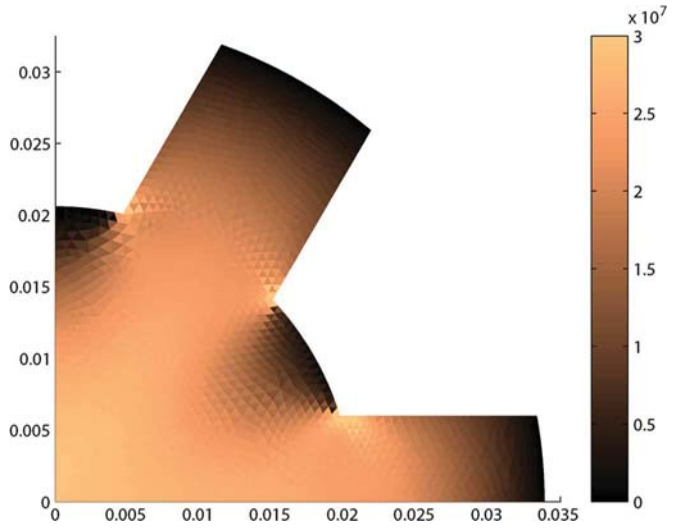

Fig. 8. Radial inertial stress σ_{rr} (Pa) in the rotor ($N = 30\,000$ rpm).

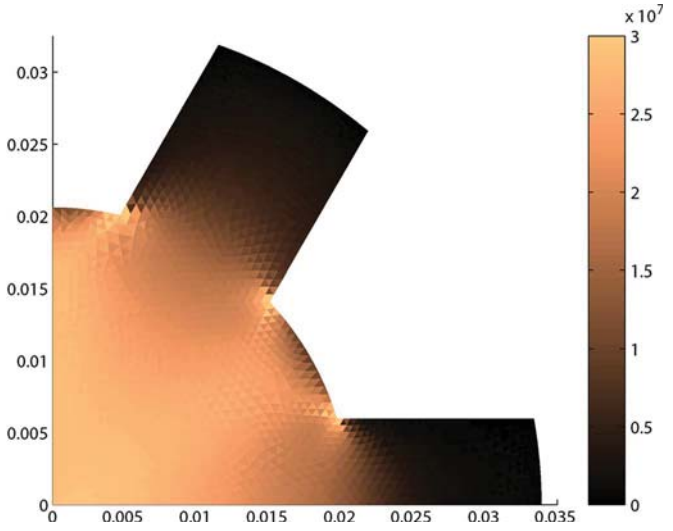

Fig. 9. Tangential inertial stress $\sigma_{\theta\theta}$ (Pa) in the rotor ($N = 30\,000$ rpm).

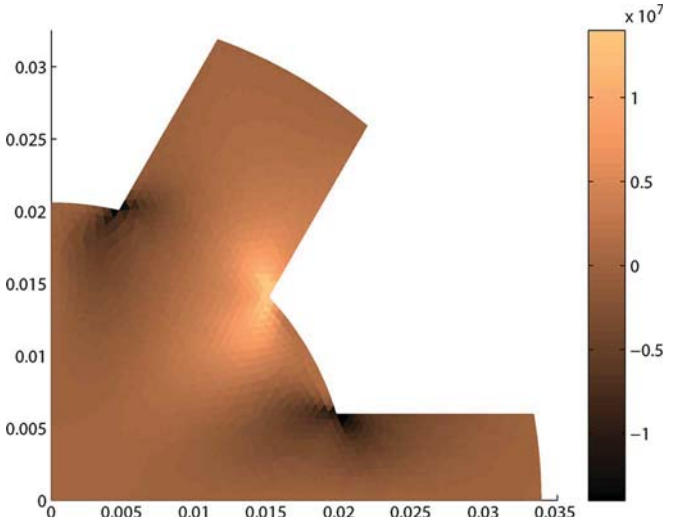

Fig. 10. Shear inertial stress $\sigma_{r\theta}$ (Pa) in the rotor ($N = 30\,000$ rpm).

each node of the mesh by derivation of the local magnetic co-energy [21]. These forces are mainly radial. The azimuthal component of these forces, that generates the torque, is small and its effect on the stress can be neglected. The radial component of the magnetic forces is taken as source term for an elastic computation on the rotor. It is found that all the components of the induced stress are lower than 2 MPa. This source of operating stress will also be neglected in the following.

Inertial stresses are the third source of operating stress. The inertial stress has been calculated and discretized according to (22) and (23). A rotational speed $N = 30\,000$ rpm ($\omega = 2\pi N/60$) has been chosen, which corresponds to a peripheral speed of 107 m/s. The density of the material is $\rho = 7800\ \mathrm{kg} \cdot \mathrm{m}^{-3}$. The inertial force density (22) leads to the expression of the external force F^{ω}

$$f = \rho\omega^2 r \tag{22}$$

$$F^{\omega} = \int_{\Omega} v f d\Omega \tag{23}$$

where v is the test function for the mechanical displacement.

The resulting distribution of inertial stress in the rotor is given in Figs. 8–10.

The stress state is mainly biaxial in the rotor, with very low shear stress, except in the lower corners of the rotor teeth. The amplitude of stress is significant (a few tens of MPa) but remains far from the yield stress of the material (about 300 MPa).

2) Initial Forces: Residual stresses arise from the forming process of the machines. These residual stresses may be due to punching, cutting, stacking, or welding processes [22], [23], [24], [25]. The estimation of these forces is very difficult since it is process dependent. However, these initial forces may significantly affect the magnetic behavior of materials. For the purpose of illustration we considered the stress resulting from the assembly process of the iron sheets. These stacking forces have been considered as a uniform compression along the z axis (orthogonal to the studied plane). This stress exists both in the stator and in the rotor and is assigned the value $\sigma_{zz} = -30$ MPa. For the practical calculation of the permeability, we consider a local coordinate system $(\vec{h}, \vec{z})$ where $\vec{h}$ is the direction of the magnetic field. The 2-D constitutive law is applied in this plane, defining the permeability in direction $\vec{h}$. This calculation is valid only if the material is initially isotropic, otherwise a full 3-D approach would be necessary.

B. *Effect of Stress on the SRM Behavior*

In order to investigate the effect of stress on the behavior of the SRM, several calculations have been carried out. The first one is a magnetic calculation without any mechanical stress. It provides the reference magnetic state of the SRM based on the magnetization curve given in Fig. 3 for a stress $\sigma = 0$. A second calculation has been done using the MSM and considering only the inertial stress at $N = 30\,000$ rpm. A third calculation has been done considering only a uniform initial compressive stress in the direction normal to the sheet plane $\sigma_{zz} = -30$ MPa. These calculations have been carried out in order to identify the most significant effects on the material permeability and on the machine torque. A full calculation with all sources of stress should be done if a design procedure is foreseen. Indeed no superimposition assumption can be made since the effect of stress on the magnetic behavior, as well as the magnetic behavior itself are strongly nonlinear.

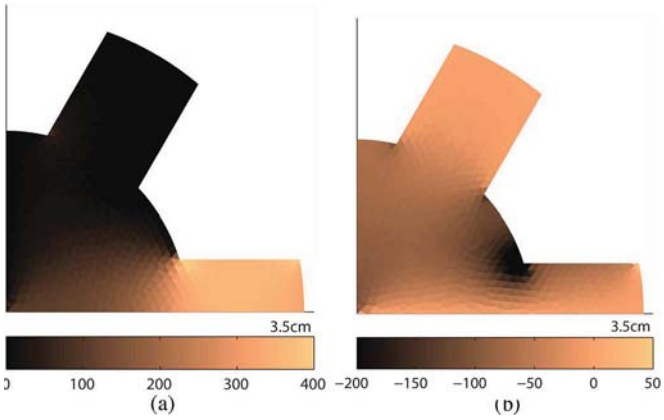

Fig. 11. Distribution of the magnetic field $(\mathrm{A}\cdot\mathrm{m}^{-1})$ in the rotor—no applied stress. (a) Radial magnetic field; (b) tangential magnetic field.

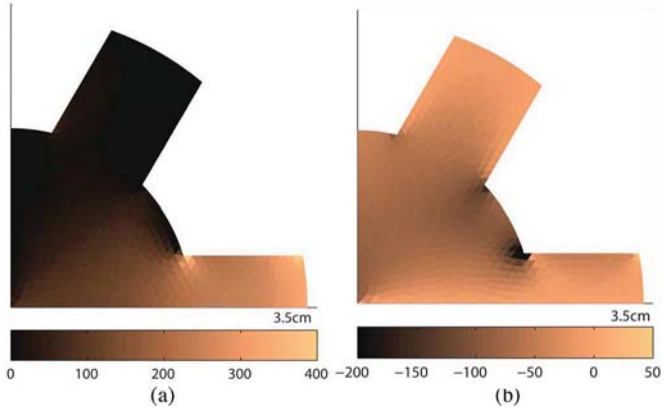

Fig. 12. Distribution of the magnetic field $(\mathrm{A}\cdot\mathrm{m}^{-1})$ in the rotor—$N = 30\,000\,\mathrm{rpm}$. (a) Radial magnetic field; (b) tangential magnetic field.

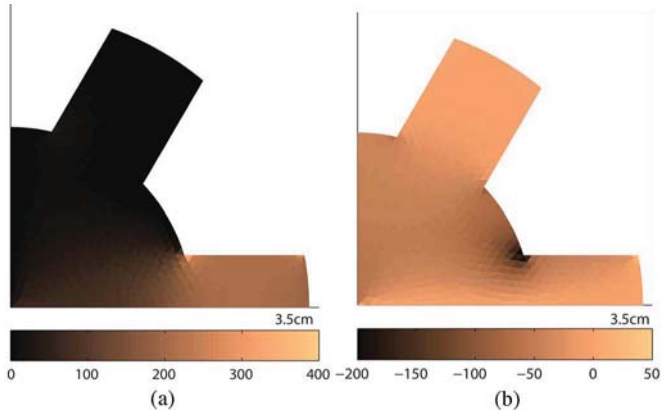

Fig. 13. Distribution of the magnetic field $(\mathrm{A}\cdot\mathrm{m}^{-1})$ in the rotor—$\sigma_{zz} = -30\ \mathrm{MPa}$. (a) Radial magnetic field; (b) tangential magnetic field.

1) Material Permeability: The effect of stress on the magnetic behavior can only be understood if the relative orientation between stress and magnetic field is known. Figs. 11–13 plot the radial and tangential components of the magnetic field in the rotor for all the considered configurations. It can be seen that the magnetic field distribution is significantly modified by the stress. The level of magnetic field (a few hundred $\mathrm{A}\cdot\mathrm{m}^{-1}$) is relatively low and remains mostly below the saturation knee of the magnetization curves (Fig. 3).

Fig. 14 plots the ratio between the predicted permeability $\mu_\sigma = \vec{B}.\vec{H}/\vec{H}^2$ considering the inertial stress and the reference

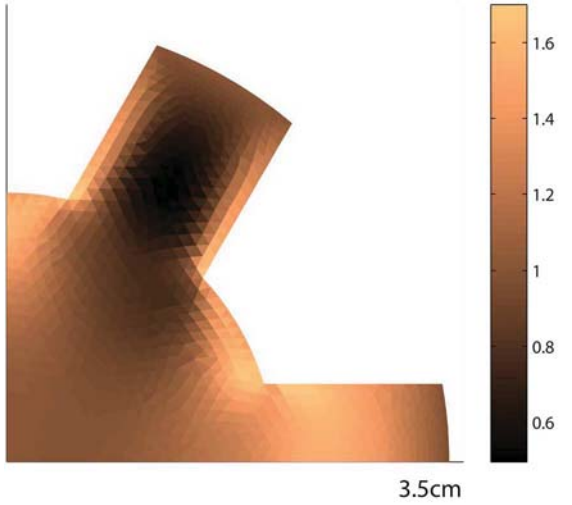

Fig. 14. Ratio μ_σ/μ_{ref} (inertial stress).

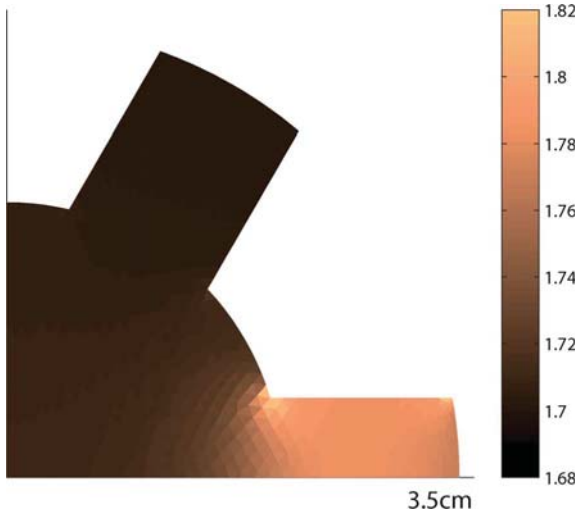

Fig. 15. Ratio $\mu_\sigma/\mu_{\mathrm{ref}}$ (initial stress $\sigma_{zz} = -30\ \mathrm{MPa}$.).

permeability μ_{ref} (with no stress). The effect of stress is very significant, as can be expected from Fig. 4. The permeability is strongly increased, up to a factor 1.7, in areas in tension with a magnetic field parallel to the stress direction. It can be divided by a factor 2 in the areas of uniaxial tension in a direction perpendicular to the magnetic field.

The same analysis is then done for the effect of the initial stress on permeability. Fig. 15 plots the ratio between the predicted permeability $\mu_\sigma = \vec{B}.\vec{H}/\vec{H}^2$ for a uniform stress $\sigma_{zz} = -30\ \mathrm{MPa}$ and the reference permeability on the rotor.

In this case, the compressive stress is normal to the magnetic field direction on the whole machine and consequently the magnetic permeability is increased up to a factor 1.8 on the rotor and the stator. The effect of stress on the permeability is non uniform owing to the non linearity of the magnetic behavior.

2) SRM Torque Calculation: A computation has been performed in order to evaluate the effect of stress on the SRM torque. A set of angular rotor positions between 0° (conjunction) and 30° is studied. The finite-element mesh includes a circular line, in the air gap, with uniform nodes density that allows to generate the different configurations without remeshing. The

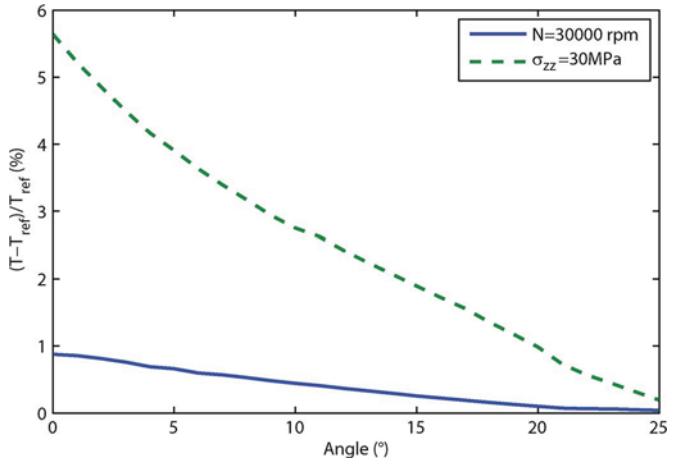

Fig. 16. Machine torque change (%) under stress.

magnetic excitation is maintained constant for all the rotor positions. The value of the torque T at each rotor position is computed from the flux of Maxwell's tensor through a circular surface γ in the air gap [21]:

$$T = r \oint_{\gamma} B_n . H_t d\gamma \tag{24}$$

where B_n and H_t are respectively the normal component of the magnetic flux density and the tangential component of the magnetic field and r the radius of γ. The relative change in the torque values under stress compared to the reference configuration is plotted in Fig. 16.

It is shown that the inertial stress has no significant influence and that the initial stress leads hardly to a 3% increase of the mean SRM torque (the mean torque values, between angular positions 2 and 20°, are respectively 16.73, 16.80, and 17.16 N·m for the configuration with no stress, with inertial stress, and with initial stress). Due to the high value of the permeability in the different cases, the torque is mainly related to the air-gap flux that is mainly controlled by the reluctivity of the air gap. Thus, the great variation of the iron reluctivity due to the stress does not significantly influence the global reluctivity of the structure.

C. Discussion

Despite the significant effect on the permeability, the calculations show that the effect of stress on the SRM torque is very narrow. The inertial stress hardly modifies the machine torque. Calculation has also been carried out for a rotational speed of 60 000 rpm with similar conclusions. Only the considered initial stress is shown to slightly modify the machine torque. A main difference between these two cases is that the initial stress modifies both the rotor and the stator permeability, affecting the whole magnetic circuit. It must be noticed that the obtained results strongly depend on the choice of motor architecture, material, and technological design—such as air-gap width. Moreover the introduction of the hysteresis in the constitutive law of the magnetic material would certainly highlight a significant effect of stress on the overall losses of the machine. This dissipative calculation is a forthcoming challenge and will be the object of further publication.

V. Conclusion

In this paper, a 2-D magneto-elastic model for the behavior of magnetic materials has been proposed. It is based on a simplification of a full multiscale approach previously proposed. This simplified magneto-elastic model has been implemented into a finite-element coupled magneto-mechanical formulation. Finally the proposed method for magneto-mechanical structural analysis has been applied to study a high rotation speed switched reluctance motor. Initial and operating forces have been considered for their effects on the machine behavior. The proposed model allows to understand how the relative configurations of stress and magnetic field modify the permeability. The considered stress and motor configuration have been shown to have slight influence on the SRM torque. The study of the effect of stress on the overall performance of electrical machine is still the object of ongoing researches, notably concerning the modeling of hysteresis losses. In this context a structural analysis tool introducing the multiaxial magneto-elastic coupling into material constitutive laws constitutes a step towards a fully coupled design of electromagnetic devices.

Appendix
Constitutive Parameter Identification for Isotropic Material

In the case of isotropic materials, the constitutive parameters for the simplified 2-D model reduce to M_s, λ and A_s.

1) M_s is the saturation magnetization of the material (this is also the case for anisotropic materials).
2) The determination of λ relies on the definition of the saturation magnetostriction strain λ_s as the difference between the strain at very high magnetic field and the strain at zero magnetic field under no applied stress:

$$\lambda_s = \varepsilon_l^{\mu}(H_{\rm sat}, \mathbf{0}) - \varepsilon_l^{\mu}(\mathbf{0}, \mathbf{0}). \tag{25}$$

The saturation state is defined as a single domain configuration with magnetization parallel to the applied field. We then have

$$\varepsilon_l^{\mu}(H_{\rm sat}, \mathbf{0}) = \lambda. \tag{26}$$

The demagnetized state is defined as a configuration for which each direction $\vec{\alpha}$ is equiprobable. The magnetostriction strain is then

$$\varepsilon_l^{\mu}(\mathbf{0}, \mathbf{0}) = \frac{1}{2\pi} \int_0^{2\pi} \frac{3}{2}\lambda \left(\cos^2\alpha - \frac{1}{3}\right) d\alpha = \frac{\lambda}{4}. \tag{27}$$

We thus obtain

$$\lambda = \frac{4}{3}\lambda_s. \tag{28}$$

3) A_s can be deduced from the initial slope χ_0 of the anhysteretic magnetization curve under no applied stress following the idea presented in [13]. The principle is to write analytically the anhysteretic curve of the unstressed

isotropic material. In this particular case, the potential energy of a domain reduces to

$$W_\alpha = W_\alpha^{mag} = -\mu_0 \vec{H}.\vec{M}_\alpha = -\mu_0 H M_s \cos\alpha. \quad (29)$$

The corresponding volumetric fraction is then

$$f_\alpha = \frac{1}{S}\exp(A_s \mu_0 H M_s \cos\alpha) \quad (30)$$

with

$$S = \int_0^{2\pi} \exp(A_s \mu_0 H M_s \cos\alpha) d\alpha. \quad (31)$$

The macroscopic magnetization M of the material (parallel to the applied field) is then written:

$$M = \int_0^{2\pi} f_\alpha M_s \cos\alpha d\alpha = \frac{M_s}{S}\int_0^{2\pi} \exp(A_s \mu_0 H M_s \cos\alpha)\cos\alpha d\alpha. \quad (32)$$

For very low applied magnetic field we can make use of the following approximation:

$$\exp(A_s \mu_0 H M_s \cos\alpha) \sim 1 + A_s \mu_0 H M_s \cos\alpha. \quad (33)$$

We then obtain

$$M \sim \frac{1}{2} A_s \mu_0 H M_s^2. \quad (34)$$

Defining the initial anhysteretic susceptibility χ_0 as the ratio between M and H for very low magnetic magnetic field, we obtain

$$A_s = \frac{2\chi_0}{\mu_0 M_s^2}. \quad (35)$$

The expression of A_s for the 2-D model is very similar to the one obtained for the full 3-D multiscale model: $A_s^{3D} = 3\chi_0/(\mu_0 M_s^2)$ [13].

The three parameters of the 2-D constitutive law in the case of isotropic materials can then be very easily identified.

ACKNOWLEDGMENT

This work was supported by ANR under Grant MAEL BLAN08-2_367373.

REFERENCES

[1] R. M. Bozorth, *Ferromagnetism*. New York: Van Norstand, 1951.
[2] M. J. Sablik and D. C. Jiles, "Coupled magnetoelastic theory of magnetic and magnetostrictive hysteresis," *IEEE Trans. Magn.*, vol. 29, no. 4, pp. 2113–2123, Jul. 1993.
[3] X. J. Zheng and X. E. Liu, "A nonlinear constitutive model for Terfenol-D rods," *J. Appl. Phys.*, vol. 97, p. 053901, 2005.
[4] O. Bottauscio, A. Lovisolo, P. E. Roccato, M. Zucca, C. Sasso, and R. Bonin, "Modeling and experimental analysis of magnetostrictive devices: From the material characterization to their dynamic behavior," *IEEE Trans. Magn.*, vol. 44, no. 11, pp. 3009–3012, Nov. 2008.
[5] D. Davino, A. Giustiniani, and C. Visone, "A magnetostrictive model with stress dependence for real-time applications," *IEEE Trans. Magn.*, vol. 44, no. 11, pp. 3193–3196, Nov. 2008.
[6] K. Kashiwaya, "Fundamentals of nondestructive measurement of biaxial stress in steel utilizing magnetoelastic effect under low magnetic field," *Jpn J. Appl. Phys.*, vol. 30, p. 2932, 1991.
[7] C. S. Schneider and J. M. Richardson, "Biaxial magnetoelasticity in steels," *J. Appl. Phys.*, vol. 53, p. 8136, 1982.
[8] M. J. Sablik, L. Riley, G. Burkhardt, H. Kwun, P. Cannel, K. Watts, and R. Langman, "Micromagnetic model for biaxial stress effects on magnetic properties," *J. Appl. Phys.*, vol. 75, p. 5673, 1994.
[9] J. Pearson, P. T. Squire, M. G. Maylin, and J. G. Gore, "Biaxial stress effects on the magnetic properties of pure iron," *IEEE Trans. Magn.*, vol. 38, no. 5, pp. 3251–3253, Sep. 2000.
[10] L. Daniel and O. Hubert, "Equivalent stress criteria for the effect of stress on magnetic behavior," *IEEE Trans. Magn.*, vol. 46, no. 8, pp. 3089–3092, Aug. 2010.
[11] W. D. Armstrong, "A directional magnetization potential based model of magnetoelastic hysteresis," *J. Appl. Phys.*, vol. 91, p. 2202, 2002.
[12] N. Buiron, L. Hirsinger, and R. Billardon, "A multiscale model for magneto-elastic couplings," *J. Phys. IV*, vol. 9, p. 187, 1999.
[13] L. Daniel, O. Hubert, N. Buiron, and R. Billardon, "Reversible magneto-elastic behavior: A multiscale approach," *J. Mech. Phys. Solids*, vol. 56, p. 1018, 2008.
[14] L. Daniel and N. Galopin, "A constitutive law for magnetostrictive materials and its application to Terfenol-D single and polycrystals," *Eur. Phys. J. Appl. Phys.*, vol. 42, p. 153, 2008.
[15] F. C. Graham, C. Mudivarthi, S. Datta, and A. B. Flatau, "Modeling of Galfenol transducer using the bidirectionally coupled magnetoelastic model," *Smart Mater. Struct.*, vol. 18, p. 104013, 2009.
[16] W. D. Armstrong, "Magnetization and magnetostriction processes in Tb(0.27-0.30)Dy(0.73-0.70)Fe(1.9-2.0)," *J. Appl. Phys.*, vol. 81, p. 2321, 1997.
[17] O. Hubert and L. Daniel, "Measurement and analytical modeling of the ΔE effect in a bulk iron-cobalt alloy," *IEEE Trans. Magn.*, vol. 46, no. 2, pp. 401–404, Feb. 2010.
[18] M. Besbes, Z. Ren, and A. Razek, "A generalized finite element model of magnetostriction phenomena," *IEEE Trans. Magn.*, vol. 37, no. 5, pp. 3324–3328, Sep. 2001.
[19] A. G. Kladas and J. A. Tegopoulos, "A new scalar potential formulation for 3-D magnetostatics necessitating no source field calculation," *IEEE Trans. Magn.*, vol. 28, no. 2, pp. 1103–1106, Mar. 1992.
[20] F. Ossart and V. Ionita, "Convergence de la méthode du point fixe modifiée pour le calcul de champ magnétique avec hystérésis," *Eur. Phys. J. Appl. Phys.*, vol. 5, pp. 63–69, 1999.
[21] J. L. Coulomb, "A methodology for the determination of global electromechanical quantities from a finite element analysis and its application to the evaluation of magnetic forces, torques and stiffness," *IEEE Trans. Magn.*, vol. MAG-19, no. 6, pp. 2514–2519, Nov. 1983.
[22] A. Schoppa, J. Schneider, and C. D. Wuppermann, "Influence of the manufacturing process on the magnetic properties of non-oriented electrical steels," *J. Magn. Magn. Mater.*, vol. 215–216, pp. 74–78, 2000.
[23] F. Ossart, E. Hug, O. Hubert, C. Buvat, and R. Billardon, "Effect of punching on electrical steels: Experimental and numerical coupled analysis," *IEEE Trans. Magn.*, vol. 36, no. 5, pp. 3137–3140, Sep. 2000.
[24] A. Schoppa, J. Schneider, C. D. Wuppermann, and T. Bakon, "Influence of welding and sticking of laminations on the magnetic properties of non-oriented electrical steels," *J. Magn. Magn. Mater.*, vol. 254–255, pp. 367–369, 2003.
[25] E. G. Araujo, J. Schneider, K. Verbeken, G. Pasquarella, and Y. Houbaert, "Dimensional effects on magnetic properties of Fe-Si steels due to laser and mechanical cutting," *IEEE Trans. Magn.*, vol. 46, no. 2, pp. 231–216, Feb. 2010.